ELSEVIER

Polymer 43 (2002) 2101–2107

polymer

www.elsevier.com/locate/polymer

Thermal reversibility in crystalline morphology of LLDPE crystallites

Joo Young Nam[a], Shigenobu Kadomatsu[a], Hiromu Saito[b,*], Takashi Inoue[c]

[a]*Department of Organic and Polymeric Materials, Tokyo Institute of Technology, 2-12-1 Ookayama, Meguro-ku, Tokyo 152-8552, Japan*
[b]*Department of Organic and Polymer Materials Chemistry, Tokyo University of Agriculture and Technology, Koganei-shi, Tokyo 184-8588, Japan*
[c]*Department of Polymer Science and Technology, Yamagata University, Jonan, Yamagata 992-8510, Japan*

Received 14 May 2001; received in revised form 28 September 2001; accepted 16 October 2001

Abstract

We investigated the temperature dependence of the crystalline morphology in linear low density polyethylene by light scattering, small-angle X-ray scattering (SAXS) and oscillating-DSC. Optical anisotropy in the spherulite, defined by model calculation of the Vv scattering pattern, and the order parameter of crystal orientation within spherulite, estimated by sharpness of the Hv scattering profile, increased in the cooling process while they decreased in the heating process. That is, the morphology is thermally reversible. The morphological change with time after the temperature drop or jump was found to be very fast in several seconds. Oscillating-DSC and SAXS results suggest that the disordering in the heating process is caused by melting of thermally unstable thin lamellae existing between the thick lamellae, which are already developed at high crystallization temperature. Thus, the thermal reversibility is ascribed to the thermally unstable thin lamellae; i.e. the thin lamellae are developed fast at wide temperature range in the cooling process and they melt fast in the heating process at the temperature close to the temperature they are developed. Owing to the fast development of the thin lamellae, the crystalline morphology obtained at high temperature cannot be frozen by quenching. © 2002 Published by Elsevier Science Ltd.

Keywords: Linear low density polyethylene; Light scattering; Thermal reversibility

1. Introduction

When polymers are crystallized, molecular chains are packed regularly to form crystalline lamellae and the crystalline lamellae grow up radially to form spherulite [1–3]. To discuss the crystalline morphology within the spherulite, transmission electron microscopy (TEM) is usually used as a powerful tool [1–13]. TEM provides the morphology on different levels of the structural hierarchy, i.e. from the lamellar level to the spherulitic architecture. However, for the TEM observation, one has to cool the specimen to room temperature after crystallization at high crystallization temperature (T_c) to carry out the pretreatment, such as permanganic etching or RuO_4 staining. If some morphological change takes place after the temperature drop from T_c to room temperature, the TEM information is not for the morphology developed at T_c but for that at room temperature.

Through our kinetic studies by light scattering on linear low density polyethylene (LLDPE) we observe that the crystalline morphology developed at high crystallization temperature could not be frozen by quenching to room temperature. This may be ascribed to the temperature dependence of the crystalline morphology demonstrated by small angle X-ray scattering (SAXS), i.e. thin lamellae are developed in the amorphous region between preexisting thick lamellae in the cooling process and the crystalline morphology is thermally reversible [14–20]. However, the thermal reversibility has not been discussed by taking into account the kinetics of the morphological change.

In this paper, the change of the crystalline morphology with temperature and the thermal reversibility in LLDPE is investigated by Hv and Vv light scatterings using CCD camera system in which the time resolved measurement is possible in millisecond order. The results are discussed by combining the SAXS and oscillating-DSC results to understand the thermal reversibility.

2. Experimental

LLDPE synthesized by methallocene catalysis was kindly supplied by Mitsubishi Chemical Co. Ltd.

A thin-layer specimen (~15 μm thick) for light scattering measurement was prepared by pressing the pellet between two cover glasses at 200 °C for 1 min. A thick specimen for SAXS was prepared by compression-molding between two

* Corresponding author. Tel.: +81-42-388-7294.
E-mail address: hsaitou@cc.tuat.ac.jp (H. Saito).

0032-3861/02/$ - see front matter © 2002 Published by Elsevier Science Ltd.
PII: S0032-3861(01)00709-1

metal plates at 200 °C for 1 min. The molded specimen was then cut into thin stripes ($16 \times 6 \times 1$ mm^3).

After the thin specimen was held at 200 °C for 3 min, it was rapidly transferred into a light scattering hot stage, set at desired crystallization temperature T_c. A polarized He–Ne gas laser of 632.8 nm wavelength was applied vertically to the film specimen. The scattered light was passed through an analyzer. We employed two optical geometries; one was the Hv geometry in which the optical axis of the analyzer was set perpendicularly to that of the polarizer, and the other was the Vv geometry with a parallel set of two axes [21]. The angular distribution of light scattering intensity was detected by a highly sensitive CCD camera with 576×382 pixels (Princeton Instruments Inc.) [22–24]. The subsequent measurement was carried out at fixed temperature. Then, another run was carried out at lower temperature. In this way, the isothermal runs were repeated at appropriate temperature interval during cooling and heating processes.

The temperature dependence of the SAXS was carried out using synchrotron radiation; beam line 3C-2 at Accelerator Laboratory, Pohang University of Science and Technology, Korea. The storage ring was operated at an energy level of 2.0 GeV. The SAXS employs a point focusing optics with a Si(111) double crystal monochromator, followed by a bent cylindrical mirror. The incident beam intensity of 0.154 nm wavelength λ was monitored by using ionization chamber for the correction of minor decrease of the primary beam intensity during the measurement. The scattered intensity was detected with a one-dimensional position sensitive proportion counter with 2048 channels (EG and G 1412XR w/OMA), and the distance between the sample and the detector was about 110 cm. The geometry was checked by a chicken tendon collagen, which gave a set of sharp diffraction corresponding to a Bragg spacing of 65.3 nm.

The scattering intensity, $I_x(q)$, was corrected for background scattering after a binomial smoothing procedure. Then the scattering intensity by thermal fluctuations was subtracted from the SAXS profile $I_x(q)$ by evaluating the slope of $I_x(q)q^4$ versus q^4 plots at wide scattering vectors q, where q is $(4\pi/\lambda)\sin\theta$, λ and θ being the wavelength and scattering angle, respectively [25]. In order to obtain the correlation function, the value of the intercept of an $I_x(q)q^4$ versus q^4 plot K was used to extrapolate the intensity $(= Kq^{-4})$ to $q = \infty$, whereas $\ln(I_x(q) - I_b)$ versus q^2 was used to extrapolate the intensity at a small q region to $q = 0$ [26].

Oscillating-DSC thermogram was measured by using Seiko Instruments Exster 6200 calibrated with standard Indium. The data were stored in Hewlett Packard 712/100 Work Station. Sinusoidal temperature rise was imposed over the conventional linear temperature rise [27–30].

$$T = T_0 + Bt - A_T \sin(\omega t) \tag{1}$$

where T_0 is the starting temperature of the scanning experiment, B is the linear heating rate, t is the time, A_T is the amplitude of the temperature oscillation, and ω is the oscillating frequency given by $2\pi/p$, p being the oscillating period. The T_0 was 20 °C, the B was 2 °C/min, the A_T was 0.5 °C, and the p was 25 s throughout this study. The total heat flow curve, which is indistinguishable for the conventional DSC, was evaluated by taking sliding averages over full cycles of oscillation for the oscillated heat flow. The reversing part of the heat flow was calculated by the Fourier-transform treatment of the oscillated heat flow. The non-reversing part of the heat flow was obtained as the difference between the total heat flow and the reversing part [27–30].

3. Results and discussion

Fig. 1 shows light scattering patterns of LLDPE under Hv and Vv modes. Four-leaf-clover type pattern was observed under Hv mode and a vertical dumbbell pattern in the Vv mode at the crystallization temperature T_c of 110 °C after crystallization at the T_c for 1 h. The results suggest that spherulites are formed and crystallites are regularly arranged along the radial direction within the spherulite [31]. When the specimen was quenched into water after crystallization at the T_c, the dumbbell type Vv pattern was split into meridional lobes and the equatorial outer lobes became stronger (Fig. 1b).

The Vv scattering pattern is theoretically described by Samuels, Yoon and Stein, Meeten and Stein et al. [32–35]

$$\begin{aligned} I_{Vv} = AV^2 \cos^2\rho_1 (3/U^3)^2 \{ & (\alpha_r - \alpha_s)(\mathrm{Si}\, U - \sin U) \\ & + (\alpha_t - \alpha_s)(2\sin U - U\cos U - \mathrm{Si}\, U) \\ & + (\alpha_r - \alpha_t)[\cos^2(\theta/2)/\cos\theta]\cos^2\mu(4\sin U \\ & - U\cos U - 3\,\mathrm{Si}\, U)\}^2 \end{aligned} \tag{2}$$

$$\cos^2\rho_1 = \cos\theta/(\cos^2\theta + \sin^2\theta\cos^2\mu)^{1/2} \tag{3}$$

where A is a proportionality factor, V is the volume of

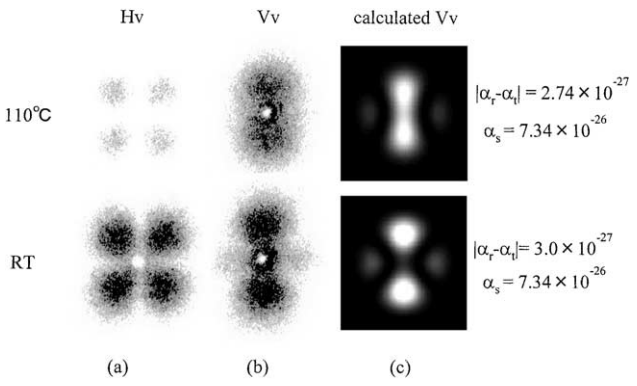

Fig. 1. Light scattering patterns of LLDPE observed at 110 °C and room temperature after full crystallization at 110 °C: (a) experimental Hv pattern, (b) experimental Vv pattern, (c) calculated Vv pattern.

spherulites, R is the radius of the spherulite, μ is the azimuthal angle, α_r and α_t are the radial and tangential polarizabilities of the spherulite, respectively, and α_s is the polarizability of the surroundings. Si U is the sine integral defined as

$$\text{Si } U = \int_0^U (\sin x/x)\mathrm{d}x \tag{4}$$

where U is given by

$$U = 4\pi(R/\lambda)\sin(\theta/2) \tag{5}$$

Since the R is fixed for the crystallized specimen (see Fig. 3), the Vv pattern can be calculated by setting values of $(\alpha_r - \alpha_t)$ and α_s by Eqs. (2)–(5).

The calculated Vv scattering patterns for various values of $(\alpha_r - \alpha_t)$ and α_s are shown in Fig. 1c. A vertical dumbbell pattern with weak equatorial outer lobes at the T_c of 110 °C in Fig. 1b is explained by setting $(\alpha_r - \alpha_t) = 2.74 \times 10^{-27}$ cm^3 and $\alpha_s = 7.34 \times 10^{-26}$ cm^3. On the other hand, four lobes pattern consisting of large meridional lobes and small equatorial ones for the quenched specimen in Fig. 1b is explained by setting $(\alpha_r - \alpha_t) = 3.0 \times 10^{-27}$ cm^3 and $\alpha_S = 7.34 \times 10^{-26}$ cm^3. This indicates that the $(\alpha_r - \alpha_t)$ at the room temperature is larger than that at the T_c. Since the $(\alpha_r - \alpha_t)$ is ascribed to the intrinsic anisotropy of the crystalline region and the orientation function for the optic axis of the crystalline region, the large anisotropy is caused by high orientation of the optical axis in the spherulite. This suggests that the ordering in the spherulite at the room temperature is larger than that at the T_c. That is, the morphology in the spherulite formed at the T_c is not frozen but is changed by quenching in spite of the full crystallization at the T_c. To understand such a morphological change, the temperature dependence of the light scattering pattern will be discussed.

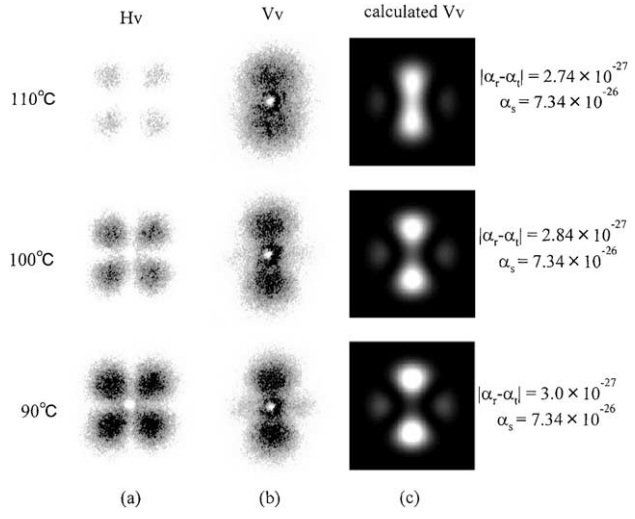

Fig. 2. Light scattering pattern of LLDPE observed in cooling process: (a) experimental Hv pattern, (b) experimental Vv pattern, (c) calculated Vv pattern.

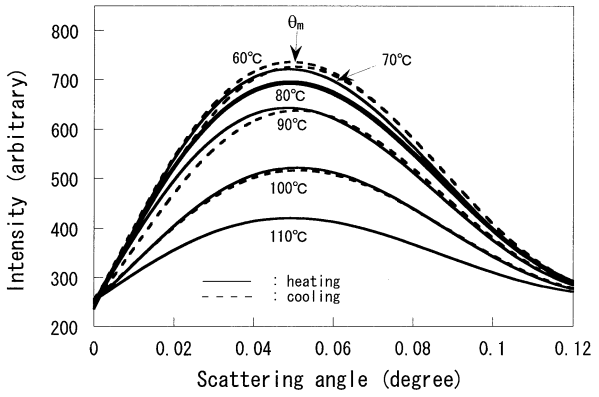

Fig. 3. Change in the Hv light scattering profiles at azimuthal angle of 45° for LLDPE crystallized at 110 °C in cooling and heating processes.

Fig. 2 shows the Hv and Vv scattering patterns for LLDPE in the cooling process after crystallization at $T_c = 110$ °C. A vertical dumbbell pattern was observed at the T_c of 110 °C. As the temperature decreased from 110 °C, the center of the dumbbell became narrower and the intensity of the equatorial lobes became stronger. The dumbbell pattern was split into two meridional lobes at around 90 °C, and then the slight change of the intensity was observed at the lower temperature.

The calculated Vv scattering patterns obtained by setting the values of $(\alpha_r - \alpha_t)$ and α_s are shown in Fig. 2c. The calculated parameter $(\alpha_r - \alpha_t)$ increases in the cooling process, suggesting that the ordering in the spherulite increases in the cooling process. The Vv scattering pattern of the quenched specimen shown in Fig. 1b is same to that observed below 90 °C. This may imply that the morphological change with temperature is so fast that the morphology is changed during the quenching and the morphology at the T_c cannot be frozen.

As shown in Fig. 2a, the intensity of the Hv scattering pattern increased in the cooling process. The one-dimensional Hv scattering profiles at an azimuthal angle of 45° in the scattering patterns of Fig. 2a is shown at various temperatures in Fig. 3. The profile has a maximum at scattering angle θ_m. The θ_m is related to the average radius of the spherulite R_s [31]:

$$4.09 = 4\pi(R_s/\lambda)\sin(\theta_m/2) \tag{6}$$

Hence, the θ_m is expected to become smaller when the R_s becomes larger. However, the θ_m was not changed with temperature, suggesting that the size of the spherulite is not changed with temperature.

Fig. 4 shows the temperature dependence of the Hv scattering intensity at θ_m obtained from Fig. 3. The intensity increased steeply in the cooling process above 90 °C and then increased gradually below 90 °C. On the other hand, the intensity decreased gradually in the heating process below 90 °C and then decreased steeply above 90 °C. The Hv scattering intensity I_{Hv} at azimuthal angle of 45° is

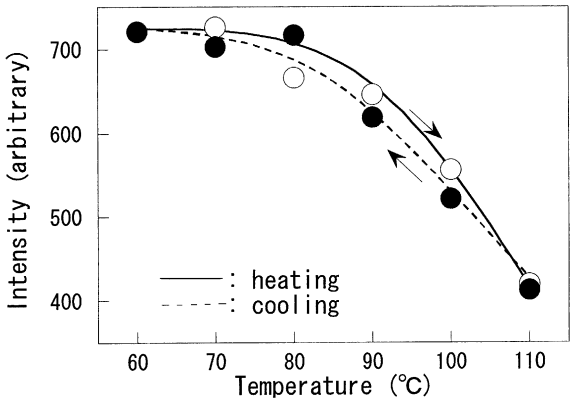

Fig. 4. Temperature dependence of Hv scattering intensity at θ_m: ●, in cooling process; ○, in heating process.

theoretically described by Stein and Rhodes [31]

$$I_{Hv} = AV^2 \cos^2 \rho_1 (3/U^3)^2 \{(\alpha_r - \alpha_t) \times [\cos^2(\theta/2)/\cos\theta] \sin\mu \cos\mu \times (4 \sin U - U \cos U - 3\,\mathrm{Si}\, U)\}^2 \quad (7)$$

Since R_s is constant, the change in the Hv intensity is mainly ascribed to that in the $(\alpha_r - \alpha_t)$. Thus the results in Fig. 4 suggest that the $(\alpha_r - \alpha_t)$ increases steeply with decreasing temperature above 90 °C and then increases gradually below 90 °C. This may support the increase of the $(\alpha_r - \alpha_t)$ in the cooling process demonstrated by Vv light scattering in Fig. 2. The intensity in the cooling process is almost same to that in the heating process, suggesting that the morphology is thermally reversible.

As shown in Fig. 3, the Hv scattering profile at high temperature was broad. The profile became sharper with decreasing temperature. According to the model calculation of the scattering profiles by Yoon and Stein [33,34], the broadening of the scattering profiles is ascribed to the orientation-angle fluctuation of the optic axis within spherulite.

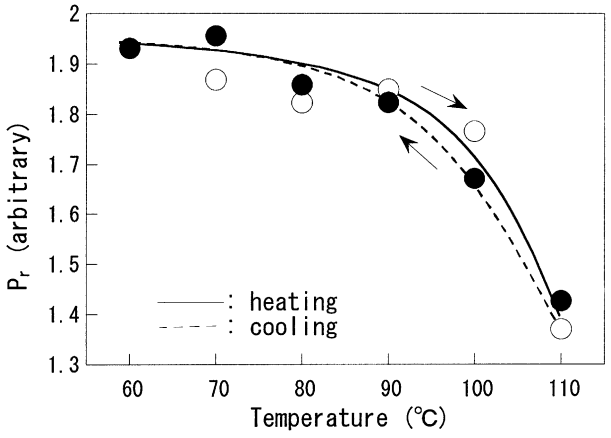

Fig. 5. Temperature dependence of the order parameter Pr: ●, in cooling process; ○, in heating process.

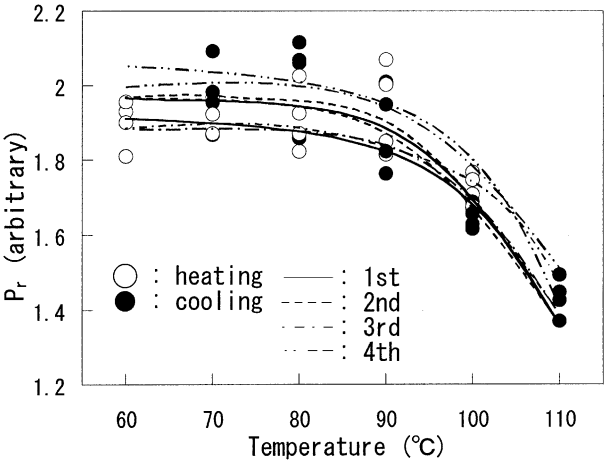

Fig. 6. Hysterisis of the order parameter Pr in cooling and heating processes.

To discuss the ordering in spherulite, we employ a ratio Pr of the intensity I at $\theta = 5°$ to that at $\theta = 10°$ because R_s is constant with temperature.

$$\mathrm{Pr} = I(\theta = 5°)/I(\theta = 10°) \quad (8)$$

Temperature dependence of the order parameter Pr in the cooling and heating processes is shown in Fig. 5. The ordering increases steeply with decreasing temperature above 90 °C and then increases gradually below 90 °C. The Pr in the cooling process is almost same to that in the heating process. The results support the change of the ordering with temperature and the thermal reversibility demonstrated before.

Fig. 6 shows the change of the Pr during the cooling and heating cycles. The Pr in the cooling process is almost same to that in the heating process at all cycles, suggesting that the morphology is thermally reversible at any heating and cooling cycles.

Fig. 7 shows the temperature dependence of the Pr in the heating process for the quenched specimen and the gradually cooled one. The temperature dependence of

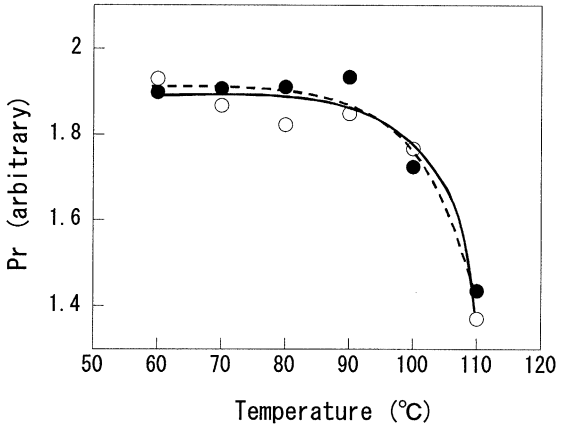

Fig. 7. Temperature dependence of the Pr in heating process: ●, quenched LLDPE; ○, gradually cooled LLDPE.

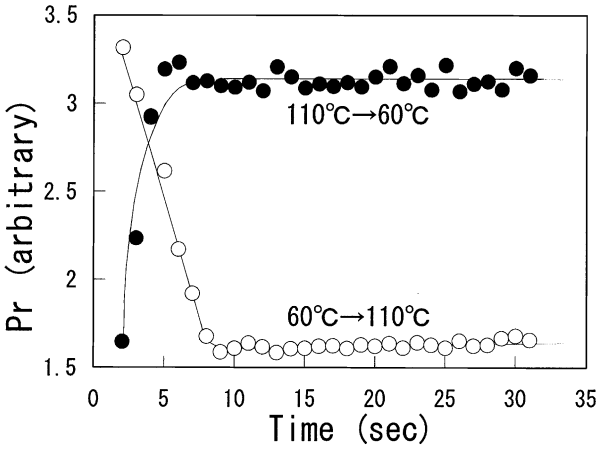

Fig. 8. Time variation of the order parameter Pr after quenching and subsequent temperature jump.

the Pr for the quenched specimen is almost same to that for the gradually cooled specimen. This suggests that the morphology of the quenched specimen is developed by the same mechanism to that of the gradually cooled specimen due to fast morphological change with temperature. Thus, the morphology changes continuously with temperature at wide temperature range during the quenching as in the case of gradual cooling.

As shown in Fig. 8, the Pr increased steeply with time after quenching from 110 to 60 °C and then leveled off at ca. 8 s. On the other hand, the Pr decreased steeply with time after the temperature jump from 60 to 110 °C and then leveled off at ca. 8 s. These results suggest that the morphological change with temperature is quite fast. This may yield the morphological change during quenching, so that the morphology obtained at the T_c cannot be frozen by quenching.

Fig. 9 shows the SAXS profiles at various temperatures in the heating process. The scattering profile shows a peak at around 0.3 nm^{-1}. The peak appears due to regular arrangement of crystalline lamellae. The peak position gradually shifts to smaller scattering vector with increasing temperature. The change is accompanied with an increase of the peak intensity. The details of morphological change will be discussed by analyzing the SAXS profiles.

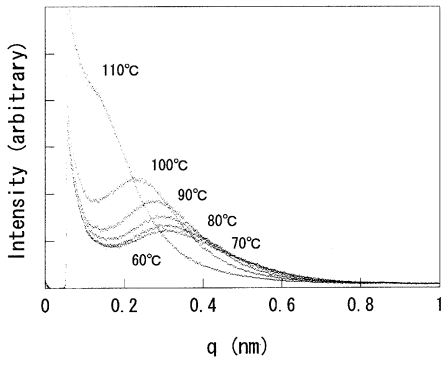

Fig. 9. SAXS profiles for various temperatures in heating process.

Several variables characterizing the lamellar morphology can be estimated from the correlation function $\gamma_1(r)$, which is given by the Fourier transform of the scattering intensity $I_x(q)$. The normalized one-dimensional correlation function is given by Strobl and Schneider [14]

$$\gamma_1(r) = \frac{1}{Q_{SAXS}} \int_0^\infty q^2 I_x(q) \cos(qr) \mathrm{d}q \tag{9}$$

$$Q_{SAXS} = \int_0^\infty q^2 I_x(q) \mathrm{d}q \tag{10}$$

where r is the coordinate along which the electron density distribution is measured.

Fig. 10 shows typical examples of the estimated $\gamma_1(r)$. The long period L, which means the most probable next-neighbor distance of the lamellae, can be determined from the position of the first maximum in the $\gamma_1(r)$. Another important parameter is the average thickness of crystalline lamellae d_c. The value of d_c can be obtained from the baseline of the first minimum in the $\gamma_1(r)$. Then, the thickness of the amorphous phase d_a is obtained by $d_a = L - d_c$.

The long period L, the lamellar thickness d_c, and the thickness of the amorphous region d_a in the heating process are shown as a function of temperature in Fig. 11. The thickness of the amorphous region d_a and that of the lamellae d_c increase gradually with increasing temperature below 90 °C and then increase steeply above 90 °C. The increase of the d_a could be ascribed to the melting of the lamellae. The increase of the d_c with temperature may be ascribed to the increase of the fraction of the thick lamellae due to the melting of the thin lamellae obtained at low temperature, as demonstrated in Refs. [15–20]. In other words, thin lamellae having various thicknesses are melted continuously with increasing temperature while thick lamellae obtained at the T_c is retained. This may imply that thin lamellae formed in the cooling process are melted continuously with increasing temperature. Thus, the increase of the ordering in the spherulite in the cooling process revealed by

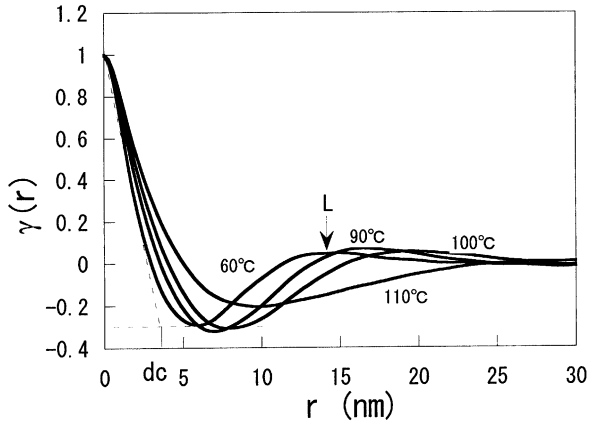

Fig. 10. One-dimensional correlation function $\gamma_1(r)$ for various temperatures in heating process.

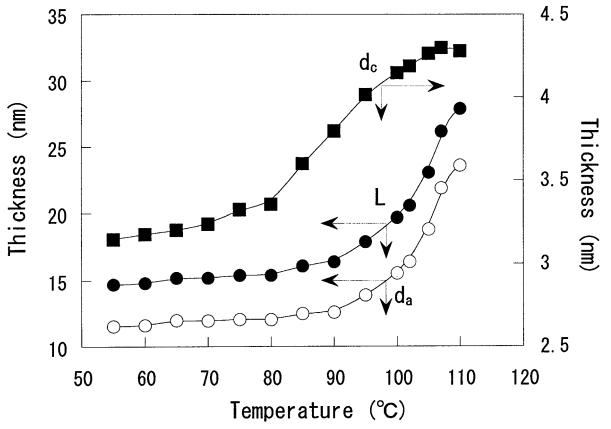

Fig. 11. Temperature dependence of long period L, thickness of crystalline lamella d_c, and thickness of amorphous region d_a in heating process.

the light scattering is ascribed to the development of the thin lamellae while the decrease of the ordering in the heating process is to the melting of the thin lamellae at the temperature close to the temperature they are developed.

Fig. 12a shows the oscillated-DSC curves of LLDPE quenched after the crystallization at 110 °C. The oscillated-DSC curves of poly(ethylene naphthalate) (PEN) quenched after the crystallization at 200 °C are also shown in Fig. 12b for comparison. The endothermic peak seen in the total heat flow is characteristic to the melting of crystallites. The peak in the total heat flow is broad for LLDPE while it is sharp for PEN. Such broad endothermic peak of LLDPE is also observed in the conventional DSC thermograms. The total heat flow can be separated into reversing and non-reversing parts [36–41]. The reversing peak is broad and large while the non-reversing peak is small and sharp in LLDPE. Hence, the broad peak in the total heat flow of LLDPE is mainly contributed by broad and large reversing peak. On the other hand, the reversing peak is small while the non-reversing peak is large and narrow in PEN. Recent oscillated-DSC studies suggest that the peak in the reversing part is ascribed to the melting of the thermally unstable poor crystallites while that in the non-reversing part to the melting of the thermally stable good crystallites [39–41]. Thus, the results suggest that large fraction of thermally unstable poor lamellae exists in LLDPE and they melt continuously at wide temperature range in the heating process, while large fraction of thermally stable good lamellae exists in PEN and they melt at narrow temperature range. This may support the melting of thin lamellae of LLDPE at wide temperature range in the heating process demonstrated by SAXS. The wide temperature range of the melting may be ascribed to broad distribution of the thickness of thermally unstable poor crystallites.

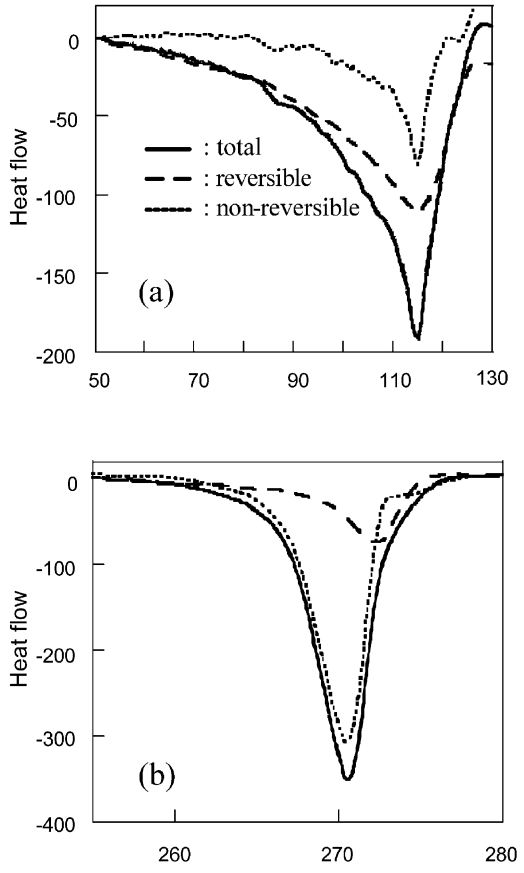

Fig. 12. Oscillating-DSC curves; (a) LLDPE, (b) PEN: (—) total heat flow, (- - -) reversing part, (···) non-reversing part.

4. Conclusion

We found that the crystalline morphology of LLDPE

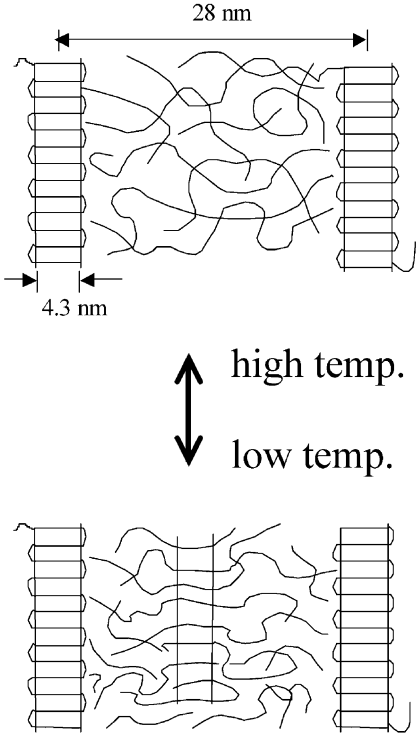

Fig. 13. Schematic drawing for the morphology change with temperature.

developed at high temperature cannot be frozen by quenching. This may be ascribed to the fast development of thermally unstable thin lamellae at wide temperature range during the quenching as in the case of gradual cooling. The thin lamellae are thermally reversible and they melt fast during the heating at narrow temperature range in which they are developed, as depicted in Fig. 13.

References

[1] Wunderlich B. Macromolecular physics. New York: Academic Press, 1973.
[2] Bassett DC. Principles of polymer morphology. Cambridge: Cambridge University Press, 1981.
[3] Barham PJ. In: Cahn RW, Hansen P, Krammer EJ, editors. Structure and properties of polymers, Materials science and technology, vol. 12. Weinheim: VCH Publishers, 1993.
[4] Grubb DT, Keller A. J Mater Sci 1972;7:822.
[5] Kanig G. Prog Colloid Polym Sci 1975;57:176.
[6] Bassett DC, Hodge AM. Polymer 1978;19:469.
[7] Sano H, Usami T, Nakagawa H. Polymer 1986;27:1497.
[8] Furuta M, Hosoda S, Kojima K. J Appl Polym Sci 1987;33:401.
[9] Hudson SD, Davis DD, Lovinger AJ. Macromolecules 1992;25:1759.
[10] Toda A, Keller A. Colloid Polym Sci 1993;271:328.
[11] Keith HD, Padden FJ. Macromolecules 1996;29:7776.
[12] Kuwabara K, Kaji H, Horii F, Bassett DC, Olley RH. Macromolecules 1997;30:7516.
[13] Takagi S, Chiba T, Saito H, Inoue T, Takemura Y. Polymer 1998;39:1643.
[14] Strobl GR, Schneider M. J Polym Sci, Polym Phys 1980;18:1343.
[15] Strobl GR, Schneider M, Voigt-Martin IG. J Polym Sci, Polym Phys 1980;18:1361.
[16] Cruz CS, Stribeck N, Zachamann HG, Calleja FJB. Macromolecules 1991;24:5980.
[17] Albrecht T, Strobl G. Macromolecules 1995;28:5267.
[18] Albrecht T, Strobl G. Macromolecules 1995;28:5827.
[19] Jonas AM, Russell TP, Yoon DY. Macromolecules 1995;28:8491.
[20] Strobl G. The physics of polymers. Berlin: Springer, 1996.
[21] Okada T, Saito H, Inoue T. Macromolecules 1992;25:1908.
[22] Lee CH, Saito H, Inoue T. Macromolecules 1993;26:6566.
[23] Lee CH, Saito H, Inoue T. Macromolecules 1995;28:8096.
[24] Lee CH, Saito H, Inoue T. Macromolecules 1996;29:7034.
[25] Koberstein JJ, Morra B, Stein RS. J Appl Crystallogr 1980;13:34.
[26] Hsiao BS, Gardner KH, Wu DQ, Chu B. Polymer 1993;34:3986.
[27] Reading M, Elliott D, Hill VL. J Therm Anal 1993;40:949.
[28] Boller A, Schick C, Wunderlich B. Thermochim Acta 1995;266:97.
[29] Schawe JEK. Thermochim Acta 1995;261:183.
[30] Takahara K, Saito H, Inoue T. Polymer 1999;40:3729.
[31] Stein RS, Rhodes MB. J Appl Phys 1960;31:1873.
[32] Samuels RJ. J Polym Sci, Part A-2 1971;9:2165.
[33] Yoon DY, Stein RS. J Polym Sci, Phys Ed 1974;12:753.
[34] Meeten GH. Optical properties of polymers. London: Elsevier, 1986.
[35] Stein RS, Misra A, Yuasa T, Khambatta F. Pure Appl Chem 1977;49:915.
[36] Wunderlich B. Macromol Symp 1995;98:1069.
[37] Okazaki I, Wunderlich B. Macromolecules 1997;30:1758.
[38] Schawe JEK, Strobl GR. Polymer 1998;39:3745.
[39] Ishikiriyama K, Wunderlich B. J Polym Sci, Part B 1997;35:1877.
[40] Cser F, Rasoul F, Kosior E. J Therm Anal 1998;52:293.
[41] Toda A, Tomita C, Hikosaka M, Saruyama Y. Polymer 1998;39:5093.